Electrostatic Layer-by-Layer Deposition and Electrochemical Characterization of Thin Films Composed of MnO 2 Nanoparticles in a Room-Temperature Ionic Liquid

ARTICLE *in* LANGMUIR · APRIL 2008

Impact Factor: 4.46 · DOI: 10.1021/la702347x · Source: PubMed

4 AUTHORS:

Tânia M Benedetti
University of Wollongong
16 PUBLICATIONS **170** CITATIONS
SEE PROFILE

Fernanda Ferraz Camilo
Universidade Federal de São Paulo
24 PUBLICATIONS **547** CITATIONS
SEE PROFILE

Eduardo Ariel Ponzio
Universidade Federal Fluminense
26 PUBLICATIONS **365** CITATIONS
SEE PROFILE

Roberto M Torresi
University of São Paulo
191 PUBLICATIONS **3,731** CITATIONS
SEE PROFILE

Electrostatic Layer-by-Layer Deposition and Electrochemical Characterization of Thin Films Composed of MnO_2 Nanoparticles in a Room-Temperature Ionic Liquid

Tânia M. Benedetti,[†] Fernanda F. C. Bazito,[‡] Eduardo A. Ponzio,[†,§] and Roberto M Torresi*,[†]

Instituto de Química, Universidade de São Paulo, CP 26077, 05513-970 São Paulo, SP, Brazil, and Departamento de Ciências Exatas e da Terra, Universidade Federal de São Paulo, Campus Diadema, 09972-270, São Paulo, SP, Brazil

Received August 1, 2007. In Final Form: December 14, 2007

Thin films of MnO_2 nanoparticles were grown using the layer-by-layer method with poly(diallyldimetylammonium) as the intercalated layer. The film growth was followed by UV−vis, electrochemical quartz crystal microbalance (EQCM), and atomic force microscopy. Linear growth due to electrostatic immobilization of layers was observed up to 30 bilayers, but electrical connectivity was maintained only for 12 MnO_2/PPDA bilayers. The electrochemical characterization of this film in 1-butyl-2,3-dimethyl-imidazolium (BMMI) bis(trifluoromethanesulfonyl)imide (TFSI) (BMMITFSI) with and without addition of a lithium salt indicated a higher electrochemical response of the nanostructured electrode in the lithium-containing electrolyte. On the basis of EQCM experiments, it was possible to confirm that the charge compensation process is achieved mainly by the TFSI anion at short times (<2 s) and by BMMI and lithium cations at longer times. The fact that large ions like TFSI and BMMI participate in the electroneutrality is attributed to the redox reaction that occurs at the superficial sites and to the high concentration of these species compared to that of lithium cations.

Introduction

Rechargeable Li-ion batteries have acquired a high commercial importance in recent years, being incorporated mainly in small mobile equipment such as cellular phones. Usually, the cathode materials for Li-ion batteries are transition metal oxides due to the high electrochemical potentials reached during reversible lithium insertion/expulsion.[1−3] Among these compounds, considerable research has been focused on manganese oxides, due to their low cost, limited environmental impact, and excellent voltage profile attributes. Despite these attractive properties, in comparison with other layered oxides ($LiCoO_2$ and $LiNiO_2$), the most used cathodic material based on manganese, $LiMn_2O_4$, presents problems related to capacity fading and limited cyclability when the potential upper limit reaches 4 V. Another detrimental feature leading to the decrease of the electrochemical performance of manganese dioxide is the dissolution of the material in contact with the electrolyte.[4−8]It is well-known that particle size and surface morphology of manganese dioxides influence their electrochemical performance.[9−15]

Besides the advantages of using nanomaterials,[16−21] the three-dimensional arrangement of these nanostructures on the electrode is also relevant. For example, it is known that layered manganese oxide thin films sometimes offer improved mechanical, catalytic, and electrochemical properties that are distinct from those of the pure nanocomponent phases and those of the related macro- and microcomposites.[22−29] However, layered manganese oxide films are difficult to obtain due to the high charge density between the active layers, which as a result have a huge tendency to agglomerate. To overcome this problem, Lvov et al.[30] recently reported the fabrication of thin films of manganese oxide with

* Corresponding author. E-mail: rtorresi@iq.usp.br. Telephone: +55 11 30912350. Fax: +55 11 38155579.

[†] Universidade de São Paulo.

[‡] Universidade Federal de São Paulo.

[§] Present address: Departamento de Físico-Química, Universidade Federal Fluminense, Campus Valonguinho, 24.020-150, Niterói (RJ), Brazil.

(1) Tarascon, J. M.; Armand, M. *Nature* **2001**, *414*, 359.
(2) Tanaka, T.; Ohta, K.; Arai, N. *J. Power Sources* **2001**, *97*−*98*, 2.
(3) Thackeray, M. M.; Ohzuku, T. *Handbook of Battery Materials*; Wiley-VCH: New York, 1999.
(4) Tarascon, J. M.; Wang, E.; Shokoohi, F. K.; Mckinnon, W. R.; Colson, S. *J. Electrochem. Soc.* **1991**, *138*, 2859.
(5) Xia, Y.; Zhou, Y.; Yoshio, M. *J. Electrochem. Soc.* **1997**, *144*, 2593.
(6) Jang, D. H.; Oh, S. M. *J. Electrochem. Soc.* **1997**, *144*, 3342.
(7) Gummov, R. J.; De Kock, A.; Thackeray, M. M. *Solid State Ionics* **1994**, *69*, 59.
(8) Bazito, F. F. C.; Torresi, R. M. *J. Braz. Chem. Soc.* **2006**, *17*, 627.
(9) Granasy, L.; Igloi, F. *J. Chem. Phys.* **1997**, *107*, 3634.
(10) Che, G.; Jirage, K. B.; Fisher, E. R.; Martin, C. R.; Yoneyama, H. *J. Electrochem. Soc.* **1997**, *144*, 4296.
(11) Patrissi, C. J.; Martin, C. R. *J. Electrochem. Soc.* **1999**, *146*, 3176.
(12) Che, G.; Lakshmi, B. B.; Fisher, E. R.; Martin, C. R. *Nature* **1998**, *393*.
(13) Kumar, R. V.; Diamant, Y.; Gedanken, A. *Chem. Mater.* **2000**, *12*, 2301.
(14) Devaraj, S.; Munichandraiah, N. *J. Electrochem. Soc.* **2007**, *154*, A80.
(15) Panigrahi, S.; Kundu, S.; Basu, S.; Praharaj, S.; Jana, S.; Pande, S.; Ghosh, S. K.; Pal, A.; Pal, T. *J. Phys. Chem. C* **2007**, *111*, 3614.
(16) Arul Dhas, N.; Koltypin, Y.; Gedanken, A. *Chem. Mater.* **1997**, *9*, 3159.
(17) Lume-Pereira, C.; Baral, S.; Henglein, A.; Janata, E. *J. Phys. Chem.* **1985**, *89*, 5772.
(18) Baral, S.; Lume-Pereira, C.; Janata, E.; Henglein, A. *J. Phys. Chem.* **1985**, *89*, 5779.
(19) Freeman, F.; Kappos, J. C. *J. Am. Chem. Soc.* **1985**, *107*, 6628.
(20) Ammundsen, B.; Jones, D. J.; Roziere, J.; Burns, G. R. *Chem. Mater.* **1997**, *9*, 3236.
(21) Sostaric, J. Z.; Mulvaney, P.; Grieser, F. *J. Chem. Soc., Faraday Trans.* **1995**, 2843.
(22) Segal, S. R.; Park, S. H.; Suib, S. L. *Chem. Mater.* **1997**, *9*, 98.
(23) Nishizawa, M.; Ise, T.; Koshika, H.; Itoh, T.; Uchida, I. *Chem. Mater.* **2000**, *12*, 1367.
(24) Long, J. W.; Qadir, L. R.; Stroud, R. M.; Rolison, D. R. *J. Phys. Chem. B* **2001**, *105*, 8712.
(25) Kanoh, H.; Tang, W.-P.; Makita, Y.; Ooi, K. *Langmuir* **1997**, *13*, 6845.
(26) Wang, P.; Zakeeruddin, S. M.; Comte, P.; Exnar, I.; Gratzel, M. *J. Am. Chem. Soc.* **2003**, *125*, 1166.
(27) Ratieuville, Y.; Wu, W.-L.; Lincot, D.; Vedel, J.; Yu, L.-T. *J. Electrochem. Soc.* **1999**, *146*, 3161.
(28) Pang, S.-C.; Anderson, M. A.; Chapman, T. W. *J. Electrochem. Soc.* **2000**, *147*, 444.
(29) Giraldo, O.; Brock, S. L.; Willis, W. S.; Marquez, M.; Suib, S. L. *J. Am. Chem. Soc.* **2000**, *122*, 9330.
(30) Lvov, Y.; Munge, B.; Giraldo, O.; Ichinose, I.; Suib, S. L.; Rusling, J. F. *Langmuir* **2000**, *16*, 8850.

10.1021/la702347x CCC: $40.75
Published on Web 02/22/2008

poly(diallyldimetylammonium) (PDDA) by a layer-by-layer technique. In the electrochemical context, the production of layered manganese oxides is important mainly due to the accommodation of the volumetric changes occurring during the redox process.[31]

In addition to the search for new electrode materials, the substitution of inflammable organic solvents commonly used in lithium-ion batteries is extremely interesting, facilitating the application of these devices in larger equipments such as electric vehicles. Another aspect of organic solvents is the difficulty of using metallic lithium as the anode, which could improve the battery's energy density. Since this metal is the most electropositive and the lightest, its use would improve the cell voltage and capacity.[32−34]

Several studies have been carried out in order to allow the use of lithium as the anode with polymeric electrolytes,[35] but these materials are restricted only to small systems because they require high temperature (80 °C) to achieve conductivity comparable to that observed with organic solvents with salts.[36,37]

Ionic liquid salts that are liquid at ambient temperature (room-temperature ionic liquids, RTILs) are good candidates for solving problems related to the use of organic solvents in batteries. They are neither flammable nor volatile, are thermally and electrochemically stable, and are highly conductive.[32−34,38−43] Nevertheless, some limitations such as high viscosity and poor wettability with electroactive materials are problems that must be overcome in order to use RTILs as electrolytes in lithium-ion batteries. The low cathodic stability of RTILs toward lithium metal is also a problem that must be faced, and many researchers are working on it.[32−34,39−41,44−57]

Several authors have studied the use of RTILs as electrolytes for different kinds of materials such as cathodic ones ($LiCoO_2$, $LiMnO_2$) or for metallic lithium.[33,34,39,58−68] Recently, Wang et al.[69] have shown that some RTILs like BMMI-TFSI, Pp14-TFSI, and TMBA-TFSI exhibit similar reactivity and are much safer than the conventional carbonate based electrolyte. Although satisfactory results have been obtained by a great number of researchers, practical applications of RTILs as electrolytes for lithium-ion batteries still seem difficult, and more research needs to be carried out in order to overcome these problems.

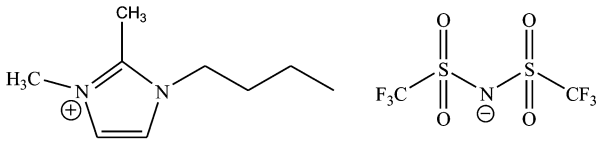

BMMI TFSI

Figure 1. Schematic structure of the 1-butyl-2,3-dimethyl-imidazolium cation, BMMI, and the bis(trifluoromethanesulfonyl)imide anion, TFSI.

In this paper, the preparation and characterization of thin films of MnO_2 nanoparticles intercalated by poly(dimethyldiallylammonium) chloride (PDDA) by using the layer-by-layer (LBL) method is presented. 1-Butyl-2,3-dimethyl-imidazolium bis(trifluoromethanesulfonyl)imide (BMMITFSI) (Figure 1) with the addition of the corresponding lithium salt was used as the electrolyte, and metallic lithium was used as counter and reference electrodes. The use of this metal was possible due to the high chemical stability of this RTIL against metallic lithium.[68] The choice of LBL methodology is due to its experimental simplicity and the preparation with success of MnO_2/PPDA thin film reported previously.[30] Used as the cathode in lithium-ion batteries, the introduction of PPDA as electrostatic glue will provide a three-dimensional molecular architecture with rigid control of thickness, grain size of the active material, morphology, and uniformity and a high degree of reproducibility. In addition, the response to substantial volumetric and/or structural changes during repeated Li^+ insertion and expulsion will also be improved due to the porosity of the film. Even though an important Mn dissolution takes place at the interface of electrode/electrolyte,[70] in this layered electrode, the concomitant insertion of the solvent will probably also occur. Thus, the bilayer deposition of PDDA will also avoid

(31) Feng, Q.; Kanoh, H.; Ooi, K. *J. Mater. Chem.* **1999**, *9*, 319.
(32) Howlett, P. C.; MacFarlane, D. R.; Hollenkamp, A. F. *Electrochem. Solid-State Lett.* **2004**, *7*, A97.
(33) Sakaebe, H.; Matsumoto, H.; Tatsumi, K. *J. Power Sources* **2005**, *146*, 693.
(34) Sakaebe, H.; Matsumoto, H. *Electrochem. Commun.* **2003**, *5*, 594.
(35) Fentone, D. E.; Parker, J. M.; Wright, P. V. *Polymer* **1973**, *14*, 589.
(36) Berthier, C.; Gorecki, W.; Minier, M.; Armand, M. B.; Chabagno, J. M.; Ruigaud, P. *Solid State Ionics* **1983**, *11*, 91.
(37) Magistris, A.; Mustarelli, P.; Quartarone, E.; Tomasi, C. *Solid State Ionics* **2000**, *136−137*, 1241.
(38) Sato, T.; Maruo, T.; Marukane, S.; Takagi, K. *J. Power Sources* **2004**, *138*, 253.
(39) Hayashi, K.; Nemoto, Y.; Akuto, K.; Sakurai, Y. *J. Power Sources* **2005**, *146*, 689.
(40) Byrne, N.; Howlett, P. C.; MacFarlane, D. R.; Forsyth, M. *Adv. Mater.* **2005**, *17*, 2497.
(41) Koch, V. R.; Nanjundiah, C.; Appetecchi, G. B.; Scrosati, B. *J. Electrochem. Soc.* **1995**, *142*, L116.
(42) Nakagawa, H.; Izuchi, S.; Kuwana, K.; Nukuda, T.; Aihara, Y. *J. Electrochem. Soc.* **2003**, *150*, A695.
(43) MacFarlane, D. R.; Meakin, P.; Sun, J.; Amini, N.; Forsyth, M. *J. Phys. Chem. B* **1999**, *103*, 4164.
(44) Suarez, P. A. Z.; Consorti, C. S.; Souza, R. F.; Dupont, J.; Gonçalves, R. S. *J. Braz. Chem. Soc.* **2002**, *13*, 106.
(45) Fuller, J.; Carlin, R. T.; Osteryoung, R. A. *J. Electrochem. Soc.* **1997**, *144*, 3881.
(46) McEwen, A. B.; Ngo, E. L.; LeCompte, K.; Goldman, J. L. *J. Electrochem. Soc.* **1999**, *146*, 1687.
(47) Koch, V. R.; Dominey, L. A.; Nanjundiah, C.; Ondrechen, M. J. *J. Electrochem. Soc.* **1996**, *143*, 798.
(48) Bonhote, P.; Dias, A.-P.; Papageorgiou, N.; Kalyanasundaram, K.; Graetzel, M. *Inorg. Chem.* **1996**, *35*, 1168.
(49) Castriota, M.; Caruso, T.; Agostino, R. G.; Cazzanelli, E.; Henderson, W. A.; Passerini, S. *J. Phys. Chem. A* **2005**, *109*, 92.
(50) Nicotera, I.; Oliviero, C.; Henderson, W. A.; Appetecchi, G. B.; Passerini, S. *J. Phys. Chem. B* **2005**, *109*, 22814.
(51) Shin, J. H.; Henderson, W. A.; Passerini, S. *Electrochem. Solid-State Lett.* **2005**, *8*, A125.
(52) Henderson, W. A.; Passerini, S. *Chem. Mater.* **2004**, *16*, 2881.
(53) Lewandowski, A.; Swiderska, A. *Solid State Ionics* **2004**, *169*, 21.
(54) McFarlane, D. R.; Sun, J.; Golding, J.; Meakin, P.; Forsyth, M. *Electrochim. Acta* **2000**, *45*, 1271.
(55) Hanabusa, K.; Fukui, H.; Suzuki, M.; Shirai, H. *Langmuir* **2005**, *21*, 10383.
(56) Matsumoto, H.; Sakaebe, H.; Tatsumi, K. *J. Power Sources* **2005**, *146*, 45.
(57) Kitaoka, S.; Nobuoka, K.; Ishikawa, Y. *Tetrahedron* **2005**, *61*, 7678.
(58) Baranchugov, V.; Markevich, E.; Pollak, E.; Salitra, G.; Aurbach, D. *Electrochem. Commun.* **2007**, *9*, 796.
(59) Seki, S.; Ohno, Y.; Kobayashi, Y.; Miyashiro, H.; Usami, A.; Mita, Y.; Tokuda, H.; Watanabe, M.; Hayamizu, K.; Tsuzuki, S.; Hattori, M.; Terada, N. *J. Electrochem. Soc.* **2007**, *154*, A173.
(60) Seki, S.; Kobayashi, Y.; Miyashiro, H.; Ohno, Y.; Usami, A.; Mita, Y.; Watanabe, M.; Terada, N. *Chem. Comm.* **2006**, 544.
(61) Egashira, M.; Tanaka-Nakagawa, M.; Watanabe, I.; Okada, S.; Yamaki, J.-i. *J. Power Sources* **2006**, *160*, 1387.
(62) Matsumoto, H.; Sakaebe, H.; Tatsumi, K.; Kikuta, M.; Ishiko, E.; Kono, M. *J. Power Sources* **2006**, *160*, 1308.
(63) Lee, S. Y.; Yong, H. H.; Kim, S. K.; Kim, J. Y.; Ahn, S. H. *J. Power Sources* **2005**, *146*, 732.
(64) Seki, S.; Kobayashi, Y.; Miyashiro, H.; Ohno, Y.; Mita, Y.; Usami, A.; Terada, N.; Watanabe, M. *Electrochem. Solid-State Lett.* **2005**, *8*, A577.
(65) Zheng, H.; Qin, J.; Zhao, Y.; Abe, T.; Ogumi, Z. *Solid State Ionics* **2005**, *176*, 2219.
(66) Zheng, H.; Li, B.; Fu, Y.; Abe, T.; Ogumi, Z. *Electrochim. Acta* **2006**, *52*, 1556.
(67) Liang, H. Y.; Qiu, X. P.; Chen, H. L.; He, Z. Q.; Zhu, W. T.; Chen, L. Q. *Electrochem. Commun.* **2004**, *6*, 789.
(68) Bazito, F. F. C.; Kawano, Y.; Torresi, R. M. *Electrochim. Acta* **2007**, *52*, 6427.
(69) Wang, Y.; Zaghib, K.; Guerfi, A.; Bazito, F. F. C.; Torresi, R. M.; Dahn, J. R. *Electrochim. Acta* **2007**, *52*, 6346.
(70) McEvoy, T. M.; Long, J. W.; Smith, T. J.; Stevenson, K. J. *Langmuir* **2006**, *22*, 4462.

the dissolution between the manganese oxide layers. Finally, although PPDA would be an isolating polymer, complete electrical contact between the active nanoparticles will probably not occur due to the linearity and flexibility of this polymer. The use of PDDA instead of other cationic polymers is due to its excellent chemical stability, its aqueous processability, and mainly its possible use in basic aqueous medium. Although lithium-ion batteries have already been extensively studied and their application in small devices established, the search for new electrodes and electrolytes (such as ionic liquids) to improve the electrochemical performance and safety is still very important. In this context, fundamental studies involving new materials with potential use in lithium-ion batteries are very relevant. Hence, the main contribution of this paper is the investigation by electrochemical quartz crystal microbalance (EQCM) of the charge compensation process of the nanostructured manganese oxide electrodes in a hydrophobic room-temperature ionic liquid. It is worth noting that there are no studies of the electroneutralization process of modified electrodes in RTIL and knowledge of the chemical nature of the species that help maintain film electroneutrality is relevant to a complete understanding of the overall electrochemical process.

Experimental

Chemical and Materials. Poly(dimethyldiallylammonium) chloride (PDDA, Aldrich) at a concentration of 2 mg mL^{-1}, pH 12 adjusted with NaOH, was used. All other chemicals were reagent grade. Potassium permanganate (99.0%), tetramethylammonium bromide (TMABr, 99.0%), mercaptoundecanoic acid (MUA), and 2-butanol (99%) were purchased from Aldrich. All chemicals were used as received without further purification.

Glass slides were cleaned by immersion in acetone for 5 min and after that rinsed with flowing water and dried under a N_2 stream.

The Au substrates were prepared by vacuum deposition of a thin layer onto Cr on quartz crystals. The freshly prepared Au substrates were immersed in a 5 mmol L^{-1} solution of MUA in ethanol for 24 h followed by thorough rinsing with ethanol to remove the excess compound.

Preparation of Manganese Dioxide via Sol−Gel. Preparation and characterization of colloids of lamellar manganese dioxide have been described in detail elsewhere.[71] Briefly, tetramethylammoniumm permanganate ($TMAMnO_4$) (1.1 mol) was prepared by dissolution of TMABr (33 mmol) in 20 mL of purified water, and then 50 mL of an aqueous solution of $KMnO_4$ (30 mmol) was added dropwise to this solution. All this was carried out with vigorous stirring of the solution. The resulting purple precipitate was filtered and recystallized from water. A colloidal solution of manganese dioxide was prepared by addition of 2 mmol of $TMAMnO_4$ in a mixture of 40 mL of purified water and 40 mL of 2-butanol at room temperature. After 45 min, a dark brown solution was obtained in the aqueous phase. The mixture was poured into a separating funnel and, after 1 h, the aqueous phase was separated. This solution was diluted with H_2O to obtain a 10^{-3} mol L^{-1} aqueous sol, which was used to deposit the MnO_2 nanoparticles onto the substrate by the LBL method. This aqueous sol is stable for a long period of time (more than 12 months) (Figure 1s, Supporting Information). In order to obtain the powder, the solution was rotary evaporated and the solid was dried in a desiccator under reduced pressure with P_2O_5 for 24 h.

Film Preparation. The $[PDDA/MnO_2]_n$ multilayers were prepared on substrates with a negative excess of charge, such as glass slides or Au covered with MUA. The films were grown by applying the LBL assembly procedure similar to that described previously.[72−74] In all cases, an upper layer of PDDA was deposited to seal the film.

Solid substrates with negative surface charge were immersed first in the PDDA solution for 10 min, then removed and washed with H_2O for 1 min, and dried under a N_2 gas flow. Afterward, they were immersed in a 10^{-3} mol L^{-1} MnO_2 aqueous solution for another 30 min and thoroughly washed with water and dried under N_2 gas flow again. Additional bilayers of $PDDA/MnO_2$ were deposited by repeating the above steps, and a multilayer film was obtained. When the assembly procedure was completed, the film electrode was dried at 45 °C under vacuum for 12 h.

Preparation of BMMITFSI. To a flask fitted with a reflux condenser was added 1.00 g (10.4 mmol) of 1,2-dimethylimidazole and 1.43 g (10.4 mmol) of butyl bromide. The mixture was stirred at 140 °C for 1 h to give a white solid. This solid was recrystallized from acetonitrile and dried under reduced pressure to give 2.29 g (95% yield) of BMMIBr as white crystals. In another flask, 250 mg (1.07 mmol) of BMMIBr was dissolved in 5.0 mL of water, and an aqueous solution of LiTFSI (308 mg, 1.07 mmol in 5.0 mL of water) was added to the flask. The reaction mixture was stirred overnight at room temperature, resulting in the formation of two separate phases. The phase containing the ionic liquid was washed several times with water, treated with activated carbon, and subjected to column chromatography (alumina, dichloromethane). The ionic liquid was dried under reduced pressure for 3 days at 100 °C to give BMMITFSI as a colorless liquid (301 mg, 0.70 mmol, 65% yield). BMMITFSI was stored in an argon atmosphere Labmaster 130 glovebox (H_2O and O_2 levels were <1 ppm). The structures of the bromide derivatives and of the ionic liquids were confirmed by ^1H and ^{13}C NMR, FTIR, and elemental analysis.[68]

Characterization Techniques. X-ray powder diffraction experiments were performed on a SIEMENS D5000 powder diffractometer using Cu Kα radiation ($\lambda = 1.5406$ Å). Field emission gun-scanning electron microscopy (FEG-SEM) analyses were run on a JEOL JSM-7401F microscope, and high-resolution transmission electron microscopy (HRTEM) experiments were performed with a JEM-3010 ARP microscope operated at 300 kV. Atomic force microscopy (AFM) topographic images were obtained using a PicoSPM-LE molecular imaging system with cantilevers operating in the intermittent-contact mode (AAC mode), slightly below their resonance frequency of approximately 305 kHz in air. All topographic images represent unfiltered original data and refer to scan areas of 50 μm × 50 μm. At least two samples of the same material were analyzed in different regions of the surface.

A HP 8452A spectrophotometer was used to obtain the UV−vis spectra, with 1.0 cm quartz cells. The sols/colloids were diluted to concentrations of $10^{-4}-10^{-5}$ mol L^{-1} Mn for the measurements. The multilayers were deposited onto the glass substrate, and the spectrum was obtained after the deposition of each bilayer.

Electrochemical Experiments. Cyclic voltammetry experiments were performed with an AUTOLAB PGSTAT 30 (Eco Chemie) equipment using platinum and lithium metallic wires as counter and reference electrodes, respectively. The working electrode was made following the procedure described above for Au electrodes. Pure BMMITFSI or BMMITFSI + 0.1 mol L^{-1} LiTFSI was used as the electrolyte. All experiments were performed in an argon atmosphere Labmaster 130 glovebox, with H_2O and O_2 concentrations below 1 ppm.

Electrochemical Quartz Crystal Microbalance. For the electrochemical quartz crystal microbalance (EQCM) experiments, the working electrode was a 6 MHz AT-cut overtone polished piezoelectric quartz crystal (Valpey-Fisher) with a diameter of 25 mm and a piezoactive electrode area of 0.31 cm^2 (integral sensitivity factor,[75] $K = 6.45 \times 10^7$ cm^2 Hz g^{-1}). Both electrode sides were previously vaporized with gold onto a chromium layer in order to improve adherence of gold onto the quartz substrate. The multilayered film was deposited on the quartz/Au electrode. The experiments were carried out in a single compartment electrochemical cell using

(71) Brock, S. L.; Sanabria, M.; Suib, S. L.; Urban, V.; Thiyagarajan, P.; Potter, D. *J. Phys. Chem. B* **1999**, *103*, 7416.
(72) Sasaki, T.; Ebina, Y.; Watanabe, M.; Decher, G. *Chem. Commun.* **2000**, 2163.
(73) Sasaki, T.; Ebina, Y.; Tanaka, T.; Harada, M.; Watanabe, M.; Decher, G. *Chem. Mater.* **2001**, *13*, 4661.
(74) Sasaki, T.; Ebina, Y.; Fukuda, K.; Tanaka, T.; Harada, M.; Watanabe, M. *Chem. Mater.* **2002**, *14*, 3524.
(75) Gabrielli, C.; Keddam, M.; Torresi, R. *J. Electrochem. Soc.* **1991**, *138*, 2657.

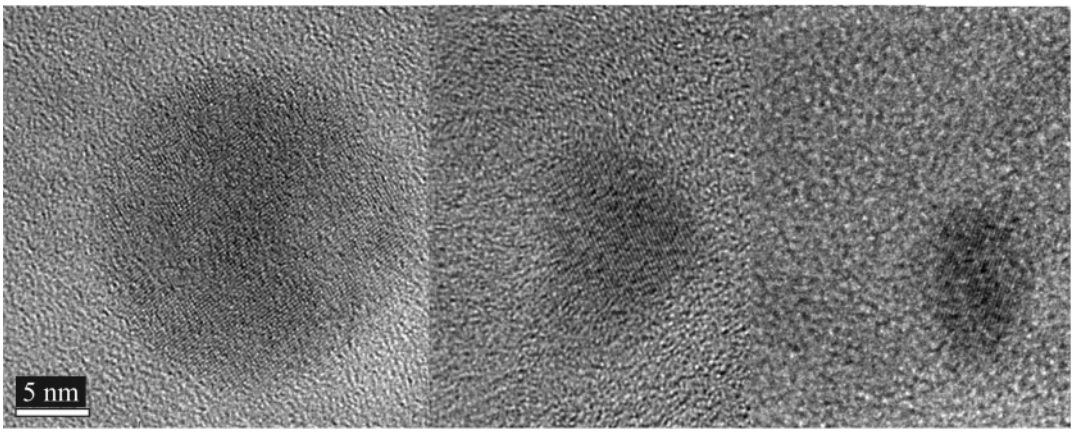

Figure 2. HRTEM images corresponding to spherical MnO_2 nanoparticles of different diameters.

Pt as the counter electrode. In all experiments, a metallic lithium wire was used as the reference electrode. Electrochemical experiments were carried out with an Omnimetra potentiostat/galvanostat model PG 3901 instrument. Frequency shifts during the potential scans were measured by using a Standford Research Systems Model SR620 instrument connected to an oscillating circuit (serial mode) and to a microcomputer for data acquisition.

Electroacoustic Impedance (EAI). EAI on the modified quartz crystals were carried out to obtain the conductance near the resonance frequency of the crystals. These measurements were made with a HP-4194A frequency impedance meter. The frequency range typically scanned in these experiments was ± 60 kHz around the fundamental resonance frequency, 6 MHz. Previous reports have detailed the dependence of the mechanical impedance of quartz crystals on both film and solution properties.[76,77] By use of homemade electrochemical cells and instrumentation, it was possible to use one face of the quartz-crystal under potential control, allowing the in situ investigation of the mechanical impedance of the MnO_2 thin films deposited onto the electrode surface.

Results and Discussion

Preparation and Characterization of the Manganese Dioxide Nanoparticles. The preparation and characterization of colloids of manganese dioxide have been already described in the literature.[71] In this work, the colloidal solutions were prepared at 10 mmol L^{-1} or lower concentrations, which stayed stable for at least 12 months in dark flasks (Figure 1s, Supporting Information).

The UV−vis spectrum of a 0.3 mmol L^{-1} solution of $TMAMnO_2$ in water presents a band at 314 nm with a broad tail in the visible region, which is responsible for the intense brown color of the material (Figure 2s, Supporting Information). These results are similar to those obtained for tetralkyllammonium manganese oxides reduced from tetralkylammonium permanganate.[71] This maximum in absorbance occurs at a lower wavelength than that observed for bulk manganese oxide, which occurs at 400 nm.[78] This suggests that the blue shift in the nanoparticle spectrum could be related to an oxidation state change of the manganese ions or a quantum size effect; however, the results are not conclusive enough to dismiss any of these possibilities.

After the removal of the solvent and the drying process, the powder obtained was analyzed by X-ray powder diffractometry. The XRD pattern corresponds to a rather amorphous material. Figure 2 shows representative HRTEM images of three MnO_2 nanoparticles. This image reveals almost spherical particles with different diameters from 20 to 5 nm. A highly ordered structure was not observed because there are several preferential directions for the atomic layers.

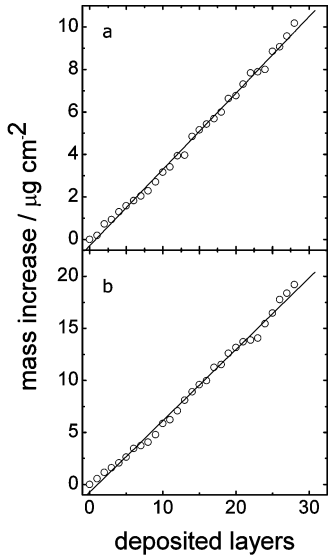

Figure 3. Mass increase as a function of the deposited layer of (a) PDDA and (b) MnO_2 nanoparticles.

LBL MnO_2 Films. Multilayer films of PDDA/MnO_2 were obtained by alternately dipping a negatively charged substrate (glass or Au/MUA) into a colloidal solution of manganese dioxide and a PDDA solution. In all films, an upper layer of PDDA was used to seal the nanoarray. The growth of the multilayers was followed by the linear increase of the absorbance at 350 nm with the number of bilayers, indicating the deposition of the same amount of material in each cycle (Figure 3s, Supporting Information). The multilayer growth was also followed by EQCM in air. By using EAI, it was confirmed that these films behave acoustically rigid, so that changes in the oscillation frequency of the EQCM can be related to mass changes by the Sauerbrey equation. Figure 3 shows the mass of PDDA (Figure 3a) and MnO_2 (Figure 3b) deposited in each bilayer. From the slopes of these plots, it was estimated that the masses of PDDA and MnO_2 per layer were 360 and 686 ng/cm^2, respectively. Upon Consideration of both sets of data, UV−vis and EQCM, it is clear that up to 30 bilayers they are physically connected to give a nanostructured electrode.

The AFM image of this film reveals a uniform and smooth surface. By this technique, it was possible to obtain direct information on the thickness of the deposited PPDA/MnO_2

(76) Hillman, A. R. *Encyclopedia of Electrochemistry*; Wiley: New York, 2003; Vol. 3, p 230.
(77) Buttry, D. A.; Ward, M. D. *Chem. Rev.* **1992**, *92*, 1355.
(78) Chen, J.; Lin, J. C.; Purhoit, V.; Cutlip, M. B.; Suib, S. L. *Catal. Today* **1997**, *33*, 205.

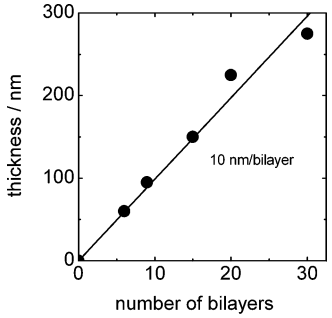

Figure 4. Film thickness determined from AFM images as a function of the number of bilayers.

bilayers. This measurement was determined from the scratch depth, intentionally made on the film surface, for different numbers of bilayers deposited on the glass substrate (Figure 4s, Supporting Information). The linear increase of the film thickness as a function of the number of bilayers is shown in Figure 4, and a thickness of 10 nm per bilayer was calculated. If we assume that the mean diameter of a nanoparticle is 10 nm and the density of the bulk MnO_2 is equal to 4 g cm^{-3}, the mass of a compact monolayer of MnO_2 should then be 1300 ng cm^{-2}. On comparison with the value obtained from the EQCM experiment (686 ng cm^{-2}), it is clear that the deposition of MnO_2 nanoparticles is spread over the entire surface.

Figure 5 shows the FEG-SEM image of a MnO_2/PDDA film (12 bilayers). It is possible to observe smooth and homogeneous nanostructured coverage, where agglomerates of 50−100 nm are present, indicating that, when the LBL film is deposited, the formation of clusters of 2−8 nanoparticles occurred.

It is possible to affirm that a diffuse structure of the electrode is obtained by taking into account the facts that the LBL deposition technique is a mild process for the immobilization of MnO_2 nanoparticles and the XRD spectrum (not shown) does not show a peak corresponding to the 001 direction, . By analyzing all experiments together (EQCM, AFM and XRD), it is possible to infer that the LBL nanoparticle film is not a perfect alternating array of MnO_2 nanoparticles and PDDA; instead, it consists of a fuzzy assembly like that schematized in Figure 6. Hence, from this point onward in the paper, the term bilayer will refer to the preparation method and not to the actual physical structure of the modified electrode.

Electrochemical Studies. The electrochemical behavior of an electrode formed by 12 bilayers of MnO_2/PDDA deposited on Au was characterized by cyclic voltammetry (CV), as shown in Figure 7, using pure BMMITFSI or BMMITFSI + 0.1 mol L^{-1} LiTFSI as the electrolyte. The reason for the use of 12 bilayers of MnO_2/PDDA will be explained in the next paragraph. In both CVs, only one redox process is observed, with anodic and cathodic current peaks at 2.2 and 1.75 V in BMMITFSI + 0.1 mol L^{-1} LiTFSI (open circles) and 2.35 and 1.60 V in BMMITFSI (open squares), respectively. Two marked differences can be observed on comparing the two CVs. The potential peak separation is greater in the case of pure BMMITFSI (0.75 V) than when LiTFSI is added (0.45 V), showing a more reversible behavior in the latter case. The other distinct aspect is the higher capacity (current density/sweep rate) observed when LiTFSI was added to the pure BMMITFSI (open circles). Charge transfer in MnO_2 is a process concomitant with cation intercalation to maintain neutrality (eq 1). It is clear that the presence of Li^+ enhances the electrochemical behavior due to its smaller size, which allows for a faster intercalation kinetics; generally, this pathway is the rate determining step.[79] It is worth noting that the peaks are not sharp or well defined, probably because of the amorphous nature of the manganese dioxide in the nanoarrays.

$$LiMnO_2 \underset{\text{discharge}}{\overset{\text{charge}}{\rightleftharpoons}} Li_{(1-x)}MnO_2 + xLi^+ + xe^- \ (0 \le x \le 1) \quad (1)$$

For the voltammogram presented in Figure 7 for RTIL + LiTFSI (open circles), the total oxidation charge was calculated to be 3.9 mC cm^{-2}, meaning that 40 nmol cm^{-2} of MnO_2 participate in the redox reaction Mn^{4+}/Mn^{3+}. Because 12 bilayers were deposited (8.2 μg cm^{-2}), the amount of MnO_2 was 95 nmol cm^{-2}; by comparing with the value determined from the voltammogram, it is clear that only half of the MnO_2 is electroactive. Results obtained with a similar system of MnO_2/PDDA bilayers[80] in which propylene carbonate/$LiClO_4$ was used as the electrolyte showed a molar ratio of 1:1, indicating that almost all the deposited MnO_2 is electroactive. On Comparison these two systems, it is clear that electroactivity is smaller in RTIL than in conventional organic solvents. There are at least two reasons to explain this fact: first, the swelling capacity of organic solvents is better than that of RTIL, and second, ion-

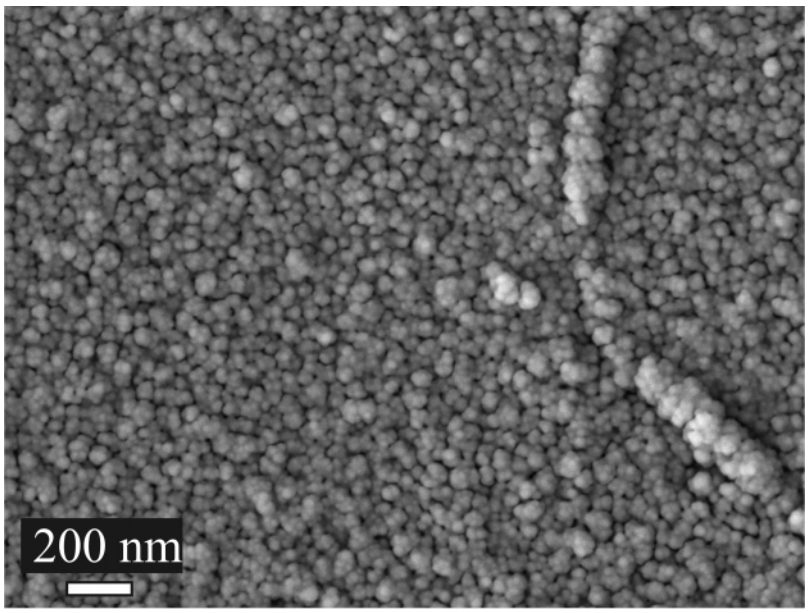

Figure 5. FEG-SEM image corresponding to the surface LBL film of 10 deposited bilayers.

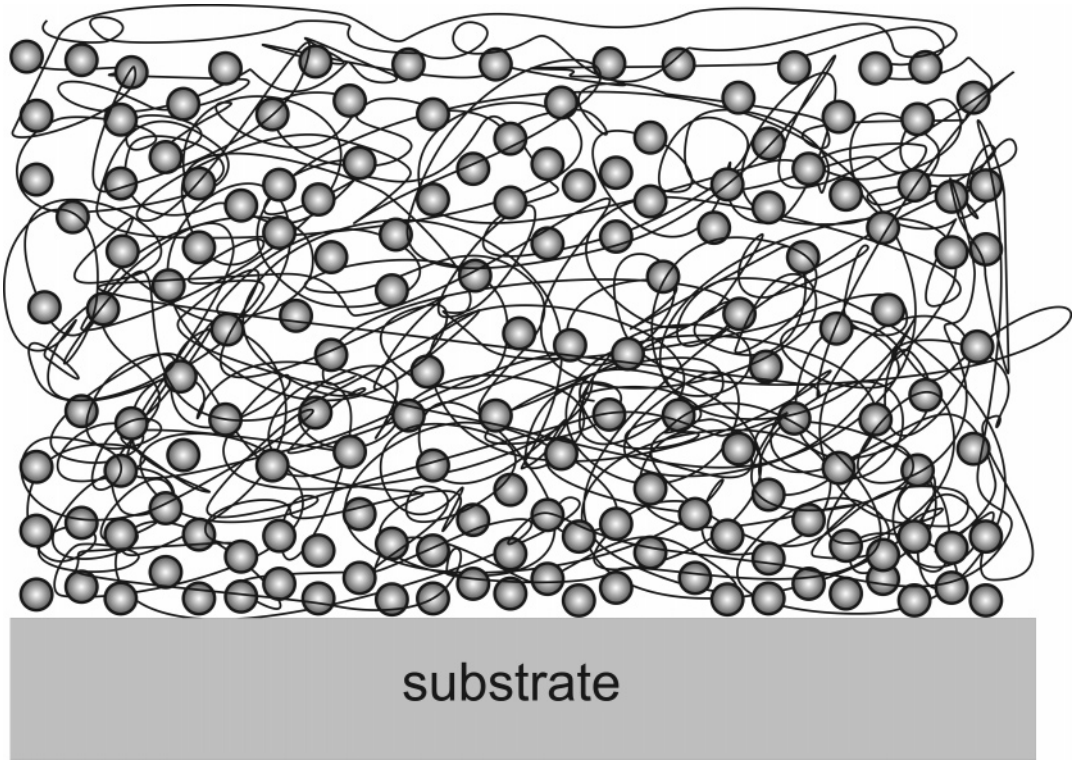

Figure 6. Scheme of the LBL film of MnO_2 nanoparticles (dark gray circles) and PDDA polyelectrolyte (gray line).

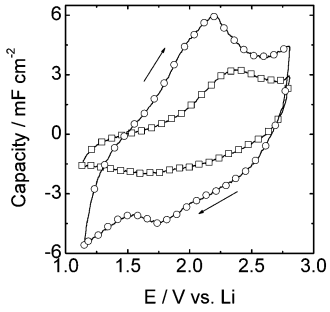

Figure 7. Potentiodynamic capacity vs *E* profiles of 12 bilayers of MnO_2/PDDA in pure BMMITFSI (open squares) and in BMMITFSI + 0.1 mol L^{-1} LiTFSI (open circles). $\upsilon = 1$ mV s^{-1}.

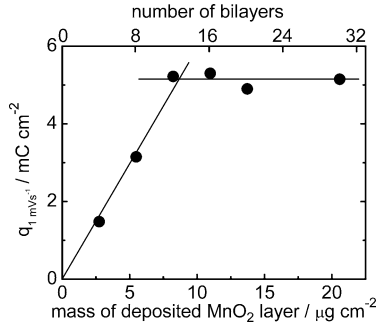

Figure 8. Charge as a function of number (mass) of bilayers of MnO_2. Anodic charges were determined from CVs carried out in BMMITFSI + 0.1 mol L^{-1} LiTFSI electrolytic solution at a sweep rate of 1 mV s^{-1}. The mass of the bilayer was determined from an EQCM experiment like that shown in Figure 3. The solid line is only to indicate the trend of charge changes.

lithium mobility (the most important characteristic of the electrolyte) is smaller in RTIL than in organic solvent due to the formation of ion-pairs and neutral aggregates.[81]

Cyclic voltammetry was also used to monitor the deposition processes of PDDA/MnO_2 bilayers and to investigate the electrical connection between the nanoparticles, i.e., to find out if all MnO_2 nanoparticles are electrically connected to the substrate. To carry out this experiment, CVs were registered after depositing bilayers of MnO_2/PDDA, and the anodic charge was calculated from the CV (at 1 mV s^{-1}) and compared with the mass calculated from EQCM experiments (Figure 3) for each bilayer. Figure 8 shows the charge for different modified electrodes (Au/(MnO_2/PDDA) as a function of the number of MnO_2 layers. Despite the increase in charge with the number of layers (or mass), which indicates the gradual increase of material on the electrode, charge values remained constant from 12 bilayers onward. This result shows that the electrical connectivity between the MnO_2 layers is only maintained up to 12 bilayers, even though it is possible to build up a modified electrode with 30 bilayers, as shown by UV−vis, EQCM, and AFM experiments. It is clear that the growth of LBL films has a limitation from the electrochemical point of view because, after several bilayers, the presence of a nonelectrically conductive polymer leads to a detrimental effect on contact between the nanoparticles and substrate. Based on this data, the modified electrode with 12 bilayers of MnO_2/PDDA was chosen as the standard one for the electrochemical measurements.

The stability of the array given by the PDDA bilayer and the seal layer is confirmed by taking into account three main aspects, which indicate and prove the absence of dissolution: first, the electrochemical response is stable for more than 100 electrochemical cycles; second, a modified electrode was left for two weeks in contact with the electrolyte and the electrochemical response was similar to the original one; and finally, UV−vis spectra of a PDDA/MnO_2 film coated on a transparent ITO electrode were recorded at several potentials, after cycles and after two weeks in contact with the electrolyte, and no significant

(79) Ponzio, E. A.; Benedetti, T. M.; Torresi, R. M. *Electrochim. Acta* **2007**, *52*, 4419.
(80) Wang, L. Z.; Omomo, Y.; Sakai, N.; Fukuda, K.; Nakai, I.; Ebina, Y.; Takada, K.; Watanabe, M.; Sasaki, T. *Chem. Mater.* **2003**, *15*, 2873.
(81) Hayamizu, K.; Aihara, Y.; Nakagawa, H.; Nukuda, T.; Price, W. S. *J. Phys. Chem. B* **2004**, *108*, 19527.

changes observed in the absorbance (see Figure 5s, Supporting Information), eliminating the possibility of dissolution of manganese species.

Another fact that needs to be analyzed is the benefit of using a nanostructured electrode with PDDA as the intercalated layer (12 bilayers). A similar mass of the same nanoparticles was deposited by the casting method, and the oxidation charge calculated from the voltammogram was approximately 40% smaller than in the case of a bilayer structured electrode. This result clearly shows that the insertion of PDDA leaves more MnO_2 sites available for the redox reaction.

EQCM and EAI Studies. It is known that EQCM is a very useful tool for simultaneously monitoring mass and charge transport in films and EAI allows the monitoring of changes in the resonance frequency of the quartz crystal produced by modifications in the bulk or interfacial properties (i.e., viscoelastic film changes or roughness modifications). Consequently, the combination of EQCM and EAI affords important information about the system, allowing one to identify the chemical nature of the ions that participate in the charge compensation process and also to raise information about the viscoelastic behavior of the films. In addition, before using the simple Sauerbrey equation to calculate mass variation from frequency changes, it is important to verify whether the thin films studied behave as an acoustically rigid system.[76,77]

EAI experiments during electrochemical perturbations were carried out to examine the changes in the mechanical properties of the material during redox cycling.[82] The following experimental protocol was used in these experiments. First, a potential of 1.7 V (reduced state, chosen as the reference state) was applied for 20 min, allowing the system to reach a steady state. This procedure was then repeated at different applied potentials to reach different oxidation states. EAI data were recorded in the 5.900 and 6.100 MHz frequency range for BMMITFSI + 0.1 mol L^{-1} LiTFSI electrolytic solution (Figure 6s, Supporting Information).

Figure 9a shows a typical conductance spectra, with a maximum at the resonance frequency, for quartz/Au in air (full line) and in the electrolytic solution (open circles). The EAI spectra can be analyzed in terms of the full width at half-maximum of the conductance peak (Δf_{fwhm}), the maximum of conductance (G_{max}), and the quality factor, which is often a useful measure of the loss of mechanical energy from the vibrating EQCM crystal to the film or solution.[76,77] The quality factor (Q) can be defined as $Q = f_o/\Delta f_{fwhm}$ (f_o is the frequency of the maximum of conductance). Figure 9a shows an important decrease in G_{max} and an increase in Δf_{fwhm} for quartz immersed in the RTIL. On Comparison of the quality factor in air (13 200) and the low values observed in the RTIL (286), the influence of the high viscosity of the RTIL is clear. A summary of the results for all the different oxidation states is shown in Figure 9b,c. No noticeable changes in the conductance or the full width at half-maximum of the conductance peak values were observed (consequently, there are also no changes in the quality factor) from the reduced to the oxidized states (Figure 9b). Specifically, the decrease in the magnitude of G_{max} is not greater than 1% and the increase in Δf_{fwhm} from 0.7 to 3.2 V was also smaller than 1%. These results point to an acoustically rigid behavior, suggesting that the resonance frequency changes between different redox states can be attributed only to mass variations. Figure 9c shows the plot of Δf_o vs the applied potential. The continuous and linear frequency increase when the film is oxidized can be interpreted as a cation expulsion from the film in order to compensate for the positive charges injected as consequence of the oxidation process. Because the

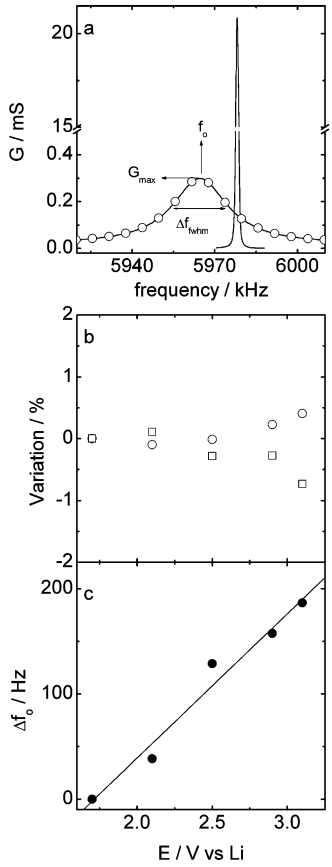

Figure 9. (a) EIA (conductance) spectrum of the quartz electrode in air (full line) and in BMMITFSI + 0.1 mol L^{-1} LiTFSI electrolytic solution (open circle). (b) Percentage variation of G_{max} (open squares) and Δf_{fwhm} (open circles). (c) Δf_o as a function of applied potential (different oxidation states) for Au/12 bilayers of MnO_2/PDDA modified electrode. The reference state used to calculate the % variation and Δf_o was the reduced one (1.7 V). Frequency sweep was 10 Hz s^{-1}.

EAI experiment indicated that the Sauerbrey equation[83] ($\Delta f = -K\Delta m$) can be employed to transform frequency variation into mass changes, a more detailed analysis of the charge compensation process was performed using EQCM.

Figure 10 shows the stationary j vs E and Δm vs E potentiodynamic profiles recorded at different sweep rates in the BMMITFSI + 0.1 mol L^{-1} LiTFSI electrolyte. The most striking feature to be noted is the dependence not only of the voltammogram but also of the mass profile on the sweep rate. From 10 to 100 mV/s, the mass behavior completely changed from a mass decrease to a mass increase during the oxidation process. Also, the higher the sweep rate the higher the participation of anions (mass increase during the oxidation process). On the basis of these results, it is possible to affirm that, at low scan rates, the charge compensation during the redox process is made by lithium cations, which are sufficiently small to move into and out of the film, and by some BMMI adsorption on the electrode surface (vide infra). At high scan rates, where the diffusion process of lithium cations is not sufficiently fast inside the film, probably only an interfacial process occurs and the adsorption/desorption of the TFSI anions takes place, a fact that explains the decrease and increase of mass during the reduction and the oxidation, respectively. This interfacial charge compensation process also explains the small electroactivity observed in the absence of LiTFSI (Figure 7, open squares).

(82) Varela, H.; Malta, M.; Torresi, R. M. *Quim. Nova* **2000**, *23*, 664.

(83) Sauerbrey, G. *Z. Phys.* **1959**, *155*, 206.

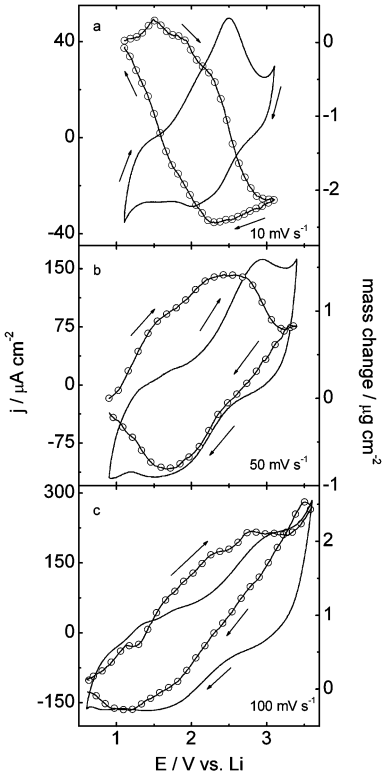

Figure 10. Potentiodynamic j vs E (full line) and Δm vs E (open circles) profiles for BMMITFSI + 0.1 mol L^{-1} LiTFSI electrolytic solution at different sweep rates: (a) 10, (b) 50, and (c) 100 mV s^{-1}.

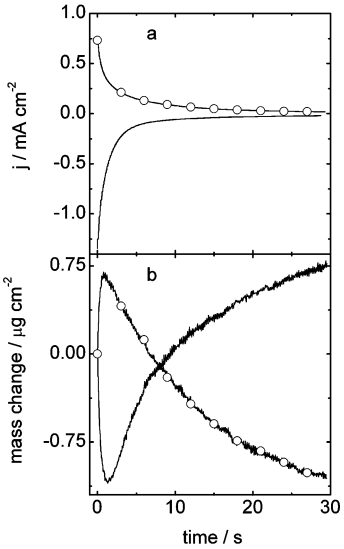

Figure 11. (a) j vs t and (b) Δm vs t profiles for a potential step from 1.85 to 2.85 V (open circle) and from 2.85 to 1.85 V (full line). BMMITFSI + 0.1 mol L^{-1} LiTFSI electrolytic solution.

In order to understand better the charge compensation process and to evaluate the bulk and interfacial contributions to the charge compensation process, an electrochemical experiment associated with EQCM was performed, adopting the following protocol. First, a potential of 1.85 V was applied for 5 min to reduce the Mn sites, reaching a steady state. Afterward, a potential step to 2.85 V was performed, and the current density and mass changes were followed as a function of time. Afterward, a potential of 1.85 V was applied, and the reduction process was also accompanied. Figure 11a shows the anodic (open circle) and cathodic (full line) current density for both potential pulses, and Figure 11b shows the mass change profiles produced during the occurrence of both processes, oxidation (open circle) and reduction (full line). At the beginning (time < 2 s), the redox process occurs at the film/electrolyte interface, and it is essentially accompanied by an increase (oxidation) or decrease (reduction) of mass, clearly indicating that TFSI anions are the main species responsible for maintaining electroneutrality. This fact was corroborated by the similarity of the molar mass of TFSI (280 g/mol) and the slope of the linear portion of the Δm versus charge plot obtained during the first 2 s (Figure 7s, Supporting Information). After 2 s, the mass starts to either diminish (oxidation) or increase (reduction), evidencing Li^+ intercalation and BMMI adsorption. This result can be rationalized in terms of the mass/charge ratio calculated from a Δm vs charge plot (Figure 6s, Supporting Information), where a slope greater than that expected for Li^+ participation but smaller than that for BMMI was obtained. Lithium cation contribution to the charge compensation process is almost completely hindered, because the molar mass of BMMI is almost 21 times greater than the molar mass of Li^+. The increase in charge capacity shown in Figure 7, where LiTFSI was added to RTIL, corroborates with lithium interaction during the redox process.

In Summary, at short times (<2 s), the TFSI participation can be understood by taking into account its higher concentration compared to Li^+ (30 times greater). However, by considering only transport properties, it is not possible to explain its participation and to exclude the BMMI, because both diffusion coefficients are very similar.[68] Probably, the more exposed negative charge on the nitrogen of TFSI explains the fast repulsion of this anion instead of BMMI approach when a negative (reduction process) charge appears on the surface of the electrode.

Previous work has shown that BMMI has a greater diffusion coefficient than Li^+[84] even though BMMI is much larger; hence, the BMMI cations arrive at the surface of the MnO_2 electrode much earlier than the highly surrounded (by TFSI anions) Li^+. This means that the BMMI barrier layer at the electrode surface against lithium-ion transportation may be formed, leading to an unfavorable impact on the kinetics of the intercalation/deintercalation reaction of lithium ion.

One suggestion to avoid the formation of a BMMI barrier at the surface of MnO_2 is to make the lithium ion move simultaneously with the cationic species of the ionic liquid in the direction of the cathode, which will then not allow the intercalation of lithium to be compromised. On the basis of these aspects, ionic liquids with cations that contain chains with oxygen substituent (ethers or crown ethers) might be interesting, since it is known that these complex strongly with lithium.

Conclusions

Ultrathin films of MnO_2 nanoparticles were grown using the layer-by-layer method and poly(diallyldimethylammonium) ions (PDDA) as the intercalated layer. UV−vis, EQCM, and AFM techniques have shown that the amount and thickness of the film increase linearly with the number of bilayers. Although the deposition is apparently uniform up to 30 bilayers, the electrical connectivity was maintained for only 12 MnO_2/PPDA bilayers. EAI experiments have also shown that, even in the presence of a highly viscous electrolyte such as BMMITFSI, the film immobilized on the substrate surface is acoustically rigid and the frequency changes produced by the redox reaction can be interpreted in terms of the Sauerbrey equation. Although the charge capacity is increased when a lithium salt is added to the RTIL, EQCM experiments showed that BMMI cations and TFSI

(84) Lee, S.-Y.; Yong, H. H.; Lee, Y. J.; Kim, S. K.; Ahn, S. *J. Phys. Chem. B* **2005**, *109*, 13663.

anions also participate in the charge compensation process, hindering the Li^+ contribution. At short times (<2 s), the participation of TFSI anions in the charge compensation process was identified. At longer times, the faster movement of BMMI forms a barrier layer on the electrode surface, leading to a detrimental effect on lithium intercalation/deintercalation kinetics.

Acknowledgment. Authors thank FAPESP (Proc. 03/10015-3), CNPq and CAPES for financial support. E.A.P. and T.M.B thank FAPESP for scholarships 01/10989-2 and 04/03411-2 and 05/59135-6, respectively. LME/LNLS (Campinas, Brazil) is gratefully acknowledged for HRTEM facilities.

Supporting Information Available: Photograph of the colloidal suspension of MnO_2, UV−vis spectra of the MnO_2 films, electrochemical quartz crystal microbalance and electroacoustic impedance data used in the present study. This material is available free of charge via the Internet at http://pubs.acs.org.

LA702347X